AUT Journal of Mechanical Engineering

AUT J. Mech. Eng., 2(2) (2018) 277-288
DOI: 10.22060/ajme.2018.14018.5698

# Modeling and Analysis of a Hybrid Photovoltaic-Thermoelectric Solar Cavity-Receiver Power Generator

O. Farhangian Marandi, M. Ameri*, B. Adelshahian

Department of Mechanical & Energy Engineering, Shahid Beheshti University, Tehran, Iran

**ABSTRACT:** In the present paper, a cavity configuration for the hybrid photovoltaic-thermoelectric generator is proposed and investigated theoretically. The cubical cavity-receiver is packed with five photovoltaic modules and four thermoelectric generator modules which are stacked at the backside of each photovoltaic module. The solution algorithm using the equations of heat transfer and generated power of photovoltaic and thermoelectric generator modules is developed via MATLAB and simulated under various irradiation levels. It is shown that under 1000 W/m$^2$ irradiation, the hybrid system can produce 536 mW which is 2.4 times the photovoltaic-thermoelectric generator alone. After modeling the system with fully open aperture, the cavity with a small aperture modeled to investigate the opening size effect on the hybrid system under non-concentrating irradiation. The results show the efficiency improvement of 27% by applying small aperture in the opening of the cavity. Although the efficiency is increased by decreasing the aperture size, the total generated power for the wide aperture is larger than the generated power in the cavity with a smaller aperture due to more radiation absorption. By balancing between minimum re-radiation loss and maximum irradiation absorption for the cubic cavity, one can conclude that the optimum aperture opening area is 42.7% of cavity surface area.

**Review History:**

Received: 28 January 2018
Revised: 4 July 2018
Accepted: 17 July 2018
Available Online: 29 July 2018

**Keywords:**

Photovoltaic-thermoelectric
Hybrid system
Solar cavity receiver
Overall efficiency
Aperture size effect

## 1- Introduction

The recent concerns about environmental issues along with the rising demand for electricity have pushed many researchers to study the new ways of harvesting renewable energies for a few decades. In the recent decade, many researchers have studied and examined PhotoVoltaic (PV) and ThermoElectric (TE) generating systems. Photovoltaic systems convert solar energy directly into electricity without having any moving part or pollution emissions. ThermoElectric Generator (TEG) is a direct energy converter device which converts thermal energy into electric power via Seebeck effect. TEG modules have no moving parts, are soundless, can also work as heat pumps which in this case they are called thermoelectric coolers and are very reliable [1]. When the PV modules are exposed to solar radiation without having any cooling system, the overall efficiency of them decreases as their temperature undesirably increases. By every degree of temperature raise the output of the PV modules decreases by about 0.5 % [2]. Therefore, the PV modules can be considered as a small degree heat source that TEG modules can be stacked on the back side of them and make a hybrid system. Many advantages make them suitable to be used with photovoltaic modules as a hybrid system.

In recent years, many researchers have studied photovoltaic-thermoelectric hybrid systems numerically and experimentally [3-6]. The concept of a coupled thermal and PV solar hybrid system was taken up in [7]. Chavez et al. [8] studied the feasibility of using thermoelectric generators in hybrid systems. Their results show, the TEG output power reached about 4% at a temperature difference of 155 °C and generated power is related to temperature difference with a power of two.

Corresponding author, E-mail: ameri_m@yahoo.com

Najafi and Woodbury [9] proposed simulation of PVT-TEG systems and the optimum required number of TEG modules for maximizing the output power and showed that the higher solar radiation level leads to higher output power by the TEG modules due to higher temperature differences. It has been shown that at a solar flux of 2800 W/m2, a hybrid system containing 36 thermoelectric modules is capable of producing 145W by a photovoltaic panel and 4.4 W by thermoelectric modules. Soltani et al. [10] tested a photovoltaic-thermoelectric hybrid system at the different cooling conditions. Natural cooling, air forced cooling, water cooling and also nanofluid cooling is applied for enhancing heat transfer of the TEG cold plate. The tests showed that using nanofluid cooling has remarkable better results for the total power of the hybrid system comparing with the air cooling methods.

In 2012, Deng et al. [11] developed and tested a hybrid system consisting of thin-film silicon cells, thermoelectric generators, and collectors. They used an integrated heat collector between the solar cell and thermoelectric module consisting optimized absorbing layer, conducting layer and an insulating layer which causes the output power for both of them to be increased. The total power of the hybrid system was twice more than that of solar cell itself. They also modeled the thermoelectric generators heat flux distribution using finite element methods and showed that much more heat is collected on the hot side of the thermoelectric module. Zhang et al. [12] studied the performance of a hybrid PV-TE system for different PV cell types at different concentrating ratios. They investigated the suitable PV cell type according to the concentration ratio and convection heat transfer factor. In case of non-concentrating irradiation, it is recommended to use polymer PV and providing a heat transfer coefficient

of around 400 W/Km2 whereas maximum efficiency occurs by using copper indium gallium selenide photovoltaic cells.
The numerical modeling of a spectrum splitting PV-TE hybrid system was presented by Ju et al. [13]. These systems comparing to the PV-only system reached to the highest efficiency as the cutoff-wavelength varies. Their results showed that the system is more suitable for working with high concentration conditions.
The three-dimensional numerical model of perovskite PV-TEG hybrid system has been studied and the results showed that the temperature coefficient of the perovskite solar cell is lower than 0.02 $^{o}K^{-1}$. This low-temperature coefficient leads to the 18.6% efficiency [14].
A hybrid photovoltaic thermoelectric system at concentrated solar irradiance by applying Fresnel lens and water heat extracting unit was studied by Willars-Rodríguez et al. [15]. This hybrid system can reach to the electrical efficiency in order of 20% and thermal efficiency of 40%.
Unlike most previous studies, Najafi and Woodbury [16] proposed a system that uses the Peltier effect to cool the photovoltaic module. The required power for the thermoelectric cooler comes from photovoltaic modules. By using the genetic algorithm optimization method, the exact supply voltage of the thermoelectric devices for reaching to optimized total power is determined.
Theoretical study of the performance of glazed/unglazed photovoltaic–thermoelectric hybrid system is presented by [17]. For enhancing heat transfer, the nanofluid is applied as a heat sink. The results showed that in the glazed system the TEG with a higher figure of merit at concentrated solar radiation is superior to the unglazed one.
In this paper, unlike the former studies, a cubical cavity, packed with photovoltaic modules and bismuth-tellurium based commercial thermoelectric devices which are placed in tandem, is proposed to study the effect of the aperture size of the cavity at various solar radiation levels on the output voltage and the current of the hybrid system. The radiation source is considered to be a metal halide lamp, and no attempt was undertaken to use concentrating tools since photovoltaic modules are sensitive to temperature raises. A heat transfer model using radiosity method is formulated to calculate the temperature distribution inside the cavity.

## 2- Theoretical Model

### 2- 1- Heat transfer model of cavity system

The schematic of solar cavity receiver configuration is shown in Fig. 1. It consists of a square parallelepiped (box) with a windowless square aperture for the access to input irradiation. The cavity contains 5 PV modules, each on every side of it and 20 TE devices that means five TE for each PV module. The conduction heat transfer through the thermoelectric legs is assumed 1D [18]. Moreover, the following assumptions are considered: (1) the PV surfaces are opaque, gray and diffuse; (2) the PV module has uniform temperatures; (3) air inside the cavity is non-participating medium in radiation (4) the PV module, and TEGs are simulated in ideal form.
One point regarding cavities is their increased apparent absorptance ($\alpha_{apparent}$) which increases the cavity ability to absorb incoming radiation. αapparent has been calculated for cylindrical, conical, and spherical geometries by many researchers [19-21]. The smaller apertures reduce re-radiation losses but intercept less sunlight, while fully open cavities

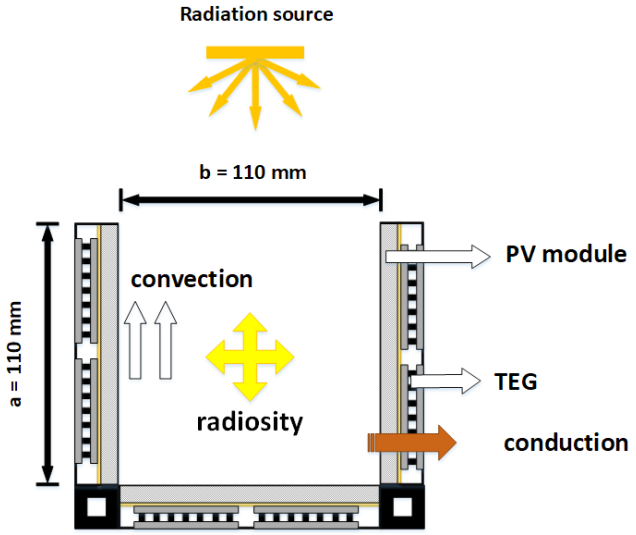


**Fig. 1. Schematic of the model domain: the cross-section of a square cavity-receiver with a windowless fully open aperture**

intercept more irradiation and also have more losses.
Fig. 2 shows αapparent as a function of the inner surface emissivity ($\varepsilon$) for a cavity size of 110×110×110 $mm^3$ with aperture width $b$ = 30, 50, 70, 90 and 110 mm. For $\alpha$ >0.65 and all aperture sizes, the αapparent is greater than 0.9.

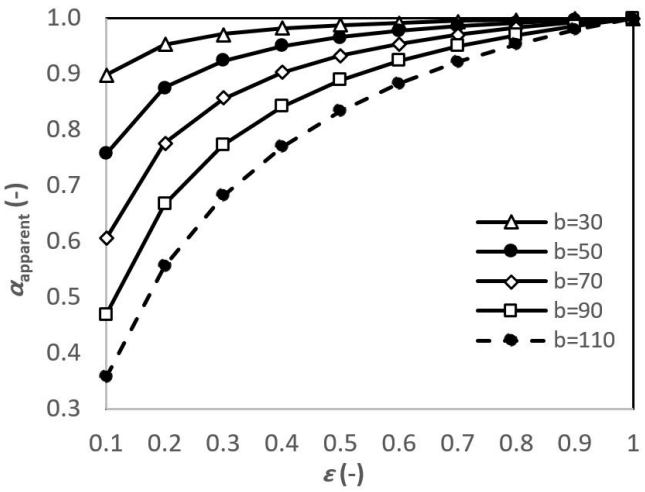


**Fig. 2. Apparent absorptance of a square box with an open aperture as a function of the absorptivity for uniformly distributed irradiation over the aperture. Baseline dimension is: $a$ = 110 mm. The parameter is the aperture width: $b$ = 30, 50, 70, 90, 110 mm (fully open aperture)**

#### 2- 1- 1- Radiation heat transfer inside the cavity

In this study, due to physical properties and working temperature of PV modules, it is assumed that the air inside the cavity does not participate in radiation exchange, and the inside surface of the cavity is gray (independent from wavelength) and diffuse. By these assumptions, the radiosity method (enclosure theory) is applied for solving the radiation heat exchange [19]. Eq. (1) is a system of formulas regarding the net radiative fluxes and temperatures of kth surface, while the surface temperature is a known parameter:

$$\varepsilon_k \cdot \sigma T^4_{1,k} = \sum_{j=1}^{N} \left[ \delta_{kj} - (1-\varepsilon_k) \cdot F_{k-j} \right] \cdot q_{o,j} \quad (1)$$

where $\varepsilon$ is surface emissivity, $\sigma$ is Stefan–Boltzmann's constant ($5.670367\times10^{-8}$ $Wm^{-2}K^{-4}$), $T_{1,k}$ is Temperature of the $k^{th}$ surface inside the cavity, $\delta$ is Kronecker delta, $F$ is view factor, and $q_o$ is radiosity flux. If the surface temperature is unknown the Eq. (2) is applied for calculating the heat flux through the walls:

$$q_k = \sum_{j=1}^{N} \left[ \delta_{kj} - F_{k-j} \right] \cdot q_{o,j} \quad (2)$$

In which $q_k$ is heat transfer through the wall which is needed to heat balance of kth surface. The cavity is discretized into six radiating surface elements. The view factors Fk-j are calculated by applying reciprocity relations $A_j F_{j-k} = A_k F_{k-j}$, enclosure criterion $\sum_{j=1}^{N} F_{k-j}=1$, and tabulated view factors for parallel and perpendicular plates [22].

The power generated by photovoltaic modules is directly dependent to irradiation level on surfaces and also their temperatures. On the other hand, the power generated by TEG module depend to inside and outside temperature of the cavity. In this study, for finding the inside cavity surface temperature, the following steps carried out:

1. Based on radiosity method, by applying a virtual surface in entrance surface, the cavity is changed to closed cavity.
2. The temperature of the aperture surface of the cavity is assumed to be zero, and so its radiosity is obtained from Eq. (1). In the first step of solving procedure, the five remaining surface temperature is unknown; therefore the radiosity of surface 2 to 5 is solved by Eq. (2). The governing equation of all surfaces radiation exchange leads to the following matrix equation, Eq. (3):

$$\begin{bmatrix} \varepsilon_1 \cdot \sigma \cdot T^4_{1,1} \\ q_2 \\ q_3 \\ q_4 \\ q_5 \\ q_6 \end{bmatrix} = \begin{bmatrix} 1-(1-\varepsilon_1)\cdot F_{1-1} & -(1-\varepsilon_1)\cdot F_{1-2} & \dots & \dots & \dots & -(1-\varepsilon_1)\cdot F_{1-6} \\ -F_{2-1} & 1-F_{2-2} & \dots & \dots & \dots & -F_{2-6} \\ -F_{3-1} & -F_{3-2} & \dots & \dots & \dots & -F_{3-6} \\ -F_{3-1} & -F_{4-2} & \dots & \dots & \dots & -F_{4-6} \\ -F_{3-1} & -F_{5-2} & \dots & \dots & \dots & -F_{5-6} \\ -F_{3-1} & -F_{6-2} & \dots & \dots & \dots & 1-F_{6-6} \end{bmatrix} \begin{bmatrix} q_{o,1} \\ q_{o,2} \\ q_{o,3} \\ q_{o,4} \\ q_{o,5} \\ q_{o,6} \end{bmatrix} \quad (3)$$

3. For solving the set of equations in Eq. (3), in the first step, it is assumed the surfaces 2 to 5 is completely insulated and so the $q_{2\text{-}5}$ is equal to zero. Solving the equations leads to the calculation of $q_{o,1\text{-}6}$ and consequently, $T_{1,1\text{-}6}$ will be found. In next step, after solving the conduction through the wall by Eq. (4) and energy balance in the cavity, the resolved temperature is used for calculating the heat flux in Eq. (3).

$$q_{cond} = \left(T_{1,k} - T_{air,out}\right) / R_{tot} \quad (4)$$

In which $T_{1,k}$ is Temperature of inside cavity surfaces, $T_{air,out}$ is outside cavity air temperature, and $R_{tot}$ is total heat resistance of PV module, TEG module, and outside air.

### 2- 1- 2- Convective heat transfer inside the cavity

During the radiation exchange between cavity surfaces, the temperatures of bottom and side surfaces increase and so the density of air which is attached to cavity walls changed and initiated the natural heat convection process inside the cavity. Based on [23], the convective heat transfer coefficient is defined as the following:

$$Nu = \exp\left(-1.736 + 0.34 ln\left(Ra\right)\right) \quad (5)$$

In which $Nu$ is the Nusselt number and $Ra$ which is the Rayleigh number is calculated as follows:

$$Ra = \frac{g.\beta}{\vartheta.\alpha}\left(T_{1,k} - T_{air,in}\right).L^3 \quad (6)$$

where $g$ is gravitational acceleration, $\beta$ is the coefficient of thermal expansion, $\vartheta$ is kinematic viscosity, $\alpha$ is thermal diffusivity, $T_{1,k}$ is the surface temperature, $T_{air,in}$ is air stream temperature inside cavity and also $L$ is characteristic length-scale of convection, in which the air properties are calculated in the air film temperature as follows [24]:

$$k_{air} = \frac{3.14\times10^{-4}.k_{air}^{0.7786}}{1-\frac{0.7116}{T_{air,in}}+\frac{2121.7}{T_{air,in}^2}} \quad (7)$$

where $k_{air}$ is air conductivity and

$$\mu_{air} = \frac{1.425*10^{-6}T^{0.5039}}{1+\frac{108.3}{T_{air,in}}} \quad (8)$$

in which $\mu_{air}$ is the air dynamic viscosity.

So the convective heat transfer inside the cavity is calculated as follow:

$$q_{conv} = h.(T_{1,k} - T_{air,in}) \quad (9)$$

The temperature of the hot side and cold side of the TEG can be found by Eqs. (10) and (11) respectively:

$$T_{2,k} = T_{1,k} - R_{pv} \cdot q_{cond} \quad (10)$$

$$T_{3,k} = T_{2,k} - R_{TEG} \cdot q_{cond} \quad (11)$$

in which $R_{pv}$ is the thermal resistance of PV module, $R_{TEG}$ is the thermal resistance of TEG module, and $q_{cond}$ is conduction heat flux.

This system of equations is solved via MATLAB for different values of solar irradiation and an ambient air temperature of 298 K.

### 2- 2- The electrical model of the hybrid system

In the next, by having the temperature values of the different points of the cavity and radiation distribution on each surface, the maximum power output from the TEGs can be found as it follows [25]:

$$P_{TEG,max} = \frac{1}{4}\frac{V_{TEG}^2}{R_i} \quad (12)$$

where $P_{TEG,max}$ is the maximum power generated by the TEG, $R_i$ is the internal electrical resistance, and $V_{TEG}$ is the open circuit of TEG module and is calculated as:

$$V_{\mathrm{TEG}} = S.\left(T_{2,k} - T_{3,k}\right) \tag{13}$$

where $S$ is the Seebeck coefficient, $T_{2,k}$ and $T_{3,k}$ are the temperatures of the hot and cold plates of the $k^{th}$ surface respectively. Furthermore, an electrical model is developed to calculate the generated power by the PV modules for any solar irradiation and cell temperature. An explicit model proposed by Saloux et al. [26] is utilized in this paper as is discussed later.

The photocurrent, as a function of irradiance and temperature, can be found as

$$I_{ph} = \frac{G}{G_{ref}}\left[I_{ph,ref} + \mu_I\left(T - T_{ref}\right)\right] \tag{14}$$

where $G_{ref}$ is the reference radiation level, $G$ is the available radiation flux on the PV module, $I_{ph,ref}$ the reference photocurrent generated by the PV module, $\mu_I$ is temperature coefficient of current, and also $T_{ref}$ is the reference temperature of PV modules. The saturation current can be written based on the short circuit current temperature coefficient and the open-circuit voltage temperature coefficient:

$$I_o = \frac{I_{sc,ref} + \mu_I\left(T - T_{ref}\right)}{\exp\left[\dfrac{q\left(V_{oc,ref} + \mu_V\left(T - T_{ref}\right)\right)}{nN_s k_B T}\right] G_{ref}} \tag{15}$$

where $I_o$ is the saturation current of the PV module, $N_s$ is the number of series PV cells, $k_B$ is $1.3806503\times10^{-23}$ $JK^{-1}$,$q$ is $1.60217646\times10^{-19}$ C , $\mu_I$=0.00045 1/°C ,$\mu_V$=0.0034 1/°C , and $n$ is the diode quality coefficient and can be determined as

$$n = \frac{q\left(V_{m,ref} + V_{oc,ref}\right)}{nN_s k_B T}\frac{1}{\ln\left(1 - \dfrac{I_{m,ref}}{I_{sc,ref}}\right)} \tag{16}$$

where $V_{m,ref}$ and $I_{m,ref}$ are the maximum voltage and current generated at the reference condition. Therefore, the voltage and current at the maximum power point and the corresponding power can be found as follows:

$$V_{mpp} = \frac{nN_s k_B T}{q}\ln\left(\frac{nN_s k_B T_1}{qI_0}\frac{I_{sc}}{V_{oc}}\right) \tag{17}$$

$$I_{mpp} = I_{ph} + I_o - \frac{nN_s k_B T_1}{q}\left(\frac{I_{sc}}{V_{oc}}\right) \tag{18}$$

$$P_{mpp} = I_{mpp} V_{mpp} \tag{19}$$

where the open circuit voltage is given as

$$V_{oc} = \frac{nN_s k_B T}{\mathrm{q}}\ln\left(1 + \frac{I_{sc}}{I_o}\right) \tag{20}$$

### 2- 3- Solution procedure

The proposed system is a hybrid system and different mechanisms of thermal heat transfer coupled with power generation by photovoltaic and thermoelectric modules that should be solved as a coupled problem. For solution of the problem, it is assumed that all of the surfaces are insulated at first, and so the heat flux is equal to zero. The upper surface temperature is the absolute zero because the surface is virtual. Moreover, it is assumed that the solar flux directly exposes to the lower surface. Afterward, by solving the Eqs. (3), (4) and (9) the temperature of the surfaces ($T_{1,k}$), the conduction through the walls ($q_{cond}$), and the amount of convective heat transfer ($q_{conv}$) in each step are calculated respectively. The temperatures of the hot and cold plates of TEG ( $T_{1,k}$ , $T_{3,k}$) are calculated by solving Eqs. (10), (11). The generated power by TEG and PV modules is calculated by Eqs. (12), (19) respectively. Solving the problem continues to achieve an error rate of less than 0.001 in the energy balance according to Eq. (21).

$$\left|\frac{Q_{solar} - Q_{reradiation} - Q_{convection} - Q_{conduction} - Q_{radiation,Out}}{Q_{solar}}\right| \le 10^{-3} \tag{21}$$

where $Q_{solar}$ is the input solar radiation to the cavity, $Q_{reradiation}$ is the re-radiation loss from the aperture, $Q_{convection}$ is the convection heat transfer by the air inside the cavity, $Q_{conduction}$ is the conduction heat transfer through the cavity walls, and $Q_{radiation,Out}$ is the radiation heat transfer from the surfaces to the outside. The steps of the solution method are given in Fig. 3.

### 2- 4- Validation of the numerical model

For validation of the numerical model, the results have been compared with PV-TEG hybrid cavity results which were investigated experimentally by Farhangian Marandi et al. [27]. They tested the 11×11×11 cm3 cavity in outdoor conditions and also laboratory conditions, at simulated irradiation 1000 ($W/m^2$). The temperature of all surface and generated power is measured and reported in [27]. The results of comparing experimental and theoretical simulations are shown in Table 1. The comparison of the results shows that the electrical power generation and temperature calculation in the present study differ less than 8% with the experimental results, which makes one confident with the expectation that the model can be used to simulate the PV-TEG cavity hybrid system.

**Table 1. Result comparison between present theoretical model and [27] in irradiation 1000($W/m^2$).**

| Case | $T_1$ (°C) | $T_2$ (°C) | $T_3$ (°C) | Total power (mW) |
|---|---|---|---|---|
| Numerical | 56.37 | 53.37 | 51.07 | 542.490 |
| Experimental[27] | 58.48 | 57.14 | 55.12 | 589.343 |
| Error (%) | 3.6 | 7.95 | 7.3 | 7.96 |

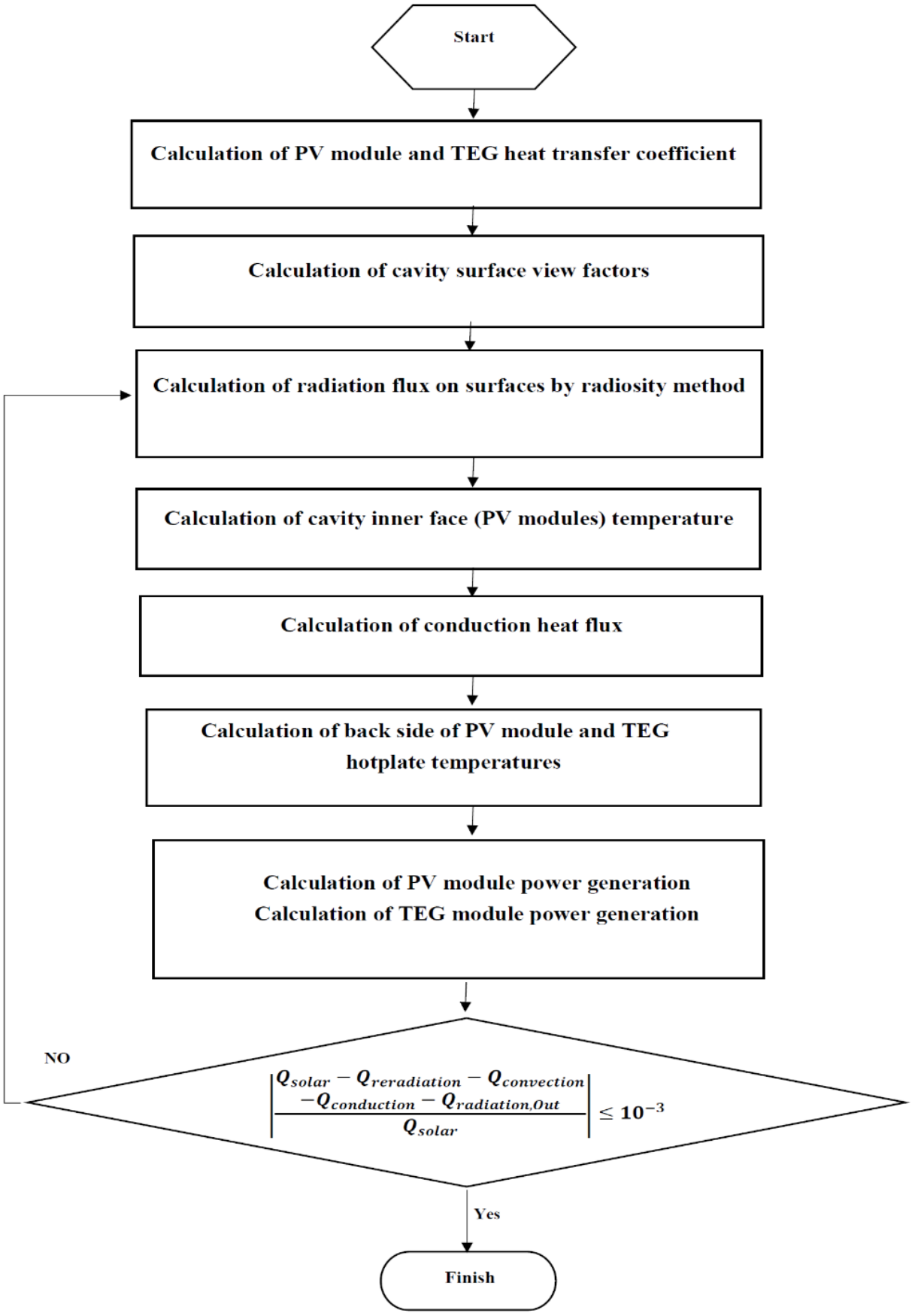


**Fig. 3. Solution procedure flowchart**

## 3- Results and Discussion

The PV module and thermoelectric generator characteristics are reported in Tables 2 and 3 respectively. The PV module properties are given in standard test conditions at irradiation of 1000 W/m$^2$ and 25˚C temperature condition.

**Table 2. PV cell characteristics (Standard Test Condition 1000W/m$^2$, 25˚C)**

| Parameter | Symbol | Value |
|---|---|---|
| Short circuit current | $I_{sc}$ (mA) | 176 |
| Open Circuit Voltage | $V_{oc}$ (V) | 6 |
| Maximum power point current | $I_{max}$ (mA) | 160 |
| Maximum power point voltage | $V_{max}$ (V) | 5.8 |
| Dimensions | $D$ (mm) | 110×110×5 |
| Maximum power | $P_{max}$ (W) | 0.92 |
| Efficiency | $\eta$ (%) | 9.8 |

In this study, the thermoelectric generator module is TGM-127 manufactured in KRYOTHERM Company, and its specifications for maximum working temperature are given in Table 3.

**Table 3. TGM-127-1,4-2,5 module specifications (T cold side =50˚C, T hot side=150 ˚C )**

| Parameter | Symbol | Value |
|---|---|---|
| Width | $W$ (mm) | 40 |
| Length | $L$ (mm) | 40 |
| Height | $H$ (mm) | 4.8 |
| Maximum voltage | $V_{max}$ (V) | 3.6 |
| Maximum current | $I_{max}$ (A) | 1.23 |
| Maximum power | $P_{max}$ (W) | 4.5 |
| Efficiency | $\eta$ (%) | 5.4 |
| Electrical resistance | $R_{elec}$ (Ω) | 3 |
| Thermal resistance | $R_{th}$ (K/W) | 2.6 |

in which $R_{elec}$ is the electric resistance of module, for specified temperature range at 1 kHz AC, $V_{max}$ is the output voltage with load resistance $R_L$=$R_{elec}$, $I_{max}$ is the output current with load resistance $R_L$=$R_{elec}$, $P_{max}$ is the output electrical power with load resistance $R_L$=$R_{elec}$, $\eta$ is the efficiency of TGM with load resistance $R_L$=$R_{elec}$ and $R_{th}$ is the internal electric resistance of TEG at working temperature.

### 3- 1- Fully open hybrid cavity

The hybrid cavity with the fully open aperture at different irradiation loads (700-1200 W/m$^2$) is simulated, and the effective parameters on the power generation rate are presented in the following figures. Figs. 4 and 5 show the variation of $T_1$ (PV module temperature), $T_2$ (TEG hot plate), and $T_3$ (TEG cold plate) versus irradiance for bottom face and the side face, respectively.

The temperatures of upside and back side of PV modules increase by raising the irradiance level. The upper limit temperature of the PV modules is about 80 °C. Therefore, the safe operation will occur at the irradiance level of 1.4 sun.

The temperature difference between $T_2$ and $T_3$ is the gradient through the TEG module, which causes power generation by

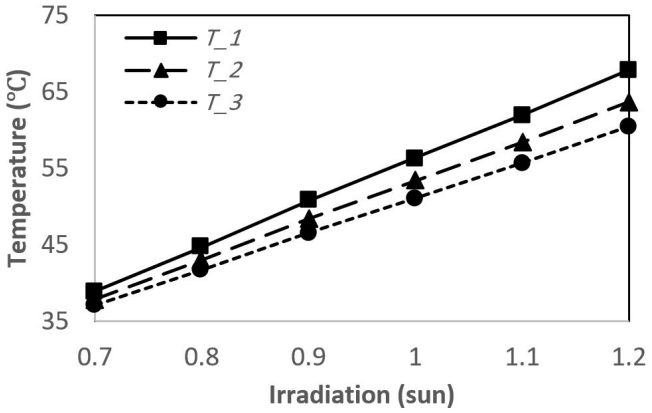


**Fig. 4. Temperature variation of PV module ($T_1$), TEG hot plate ($T_2$), and TEG cold plate ($T_3$) of the bottom face at various solar radiation levels**

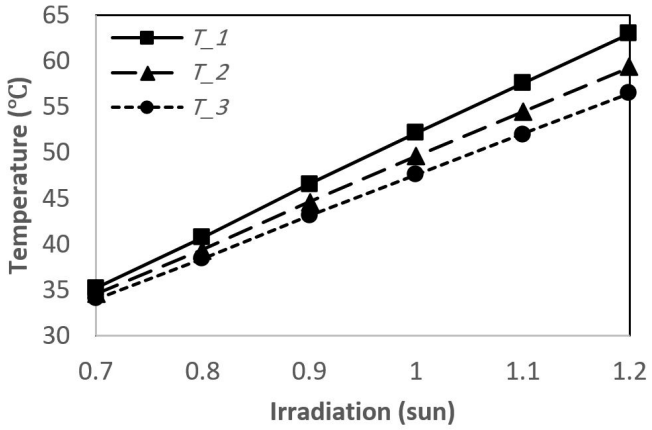


**Fig. 5. Temperature variation of PV module ($T_1$), TEG hot plate ($T_2$), and TEG cold plate ($T_3$) of the side face at various solar radiation levels**

the TEG module. The figures show that increase in irradiance level leads to higher temperature difference through the TEG and, consequently, more output power. However, by increasing the irradiance level, the PV module temperature grow rapidly, which necessitates using active cooling systems such as forced convection or using water flow through small pipes sticks at the back of the TEG modules. Applying the cooling system for TEGs allow more output power generation but increase the produced electricity costs. In this work, no particular cooling system is considered for the TEG modules and natural convection on the TEG backside surface.

The variation of the maximum generated power via the PV modules and via the four TEG modules on each side and also the total maximum power generated by the 5 PV modules and 20 TEG modules versus irradiation are given in Figs. 6 and 7, respectively. It is shown in Fig. 6 that by increasing the irradiance level, the generated power would also increase. If a higher level of irradiation exposes to the bottom side PV module, its generated power will be more than the side PV modules. Increasing the irradiation absorption by downside surface leads to the temperature enhancement, and consequently, TEG modules follow the similar trend in power generation as shown in Fig. 7.

Fig. 6 demonstrates the generated power by TEG modules.

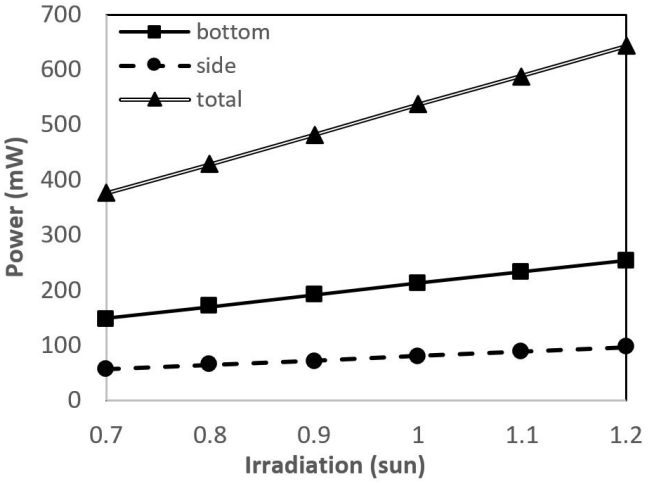


**Fig. 6. Maximum generated power by the PV modules at various radiation levels**

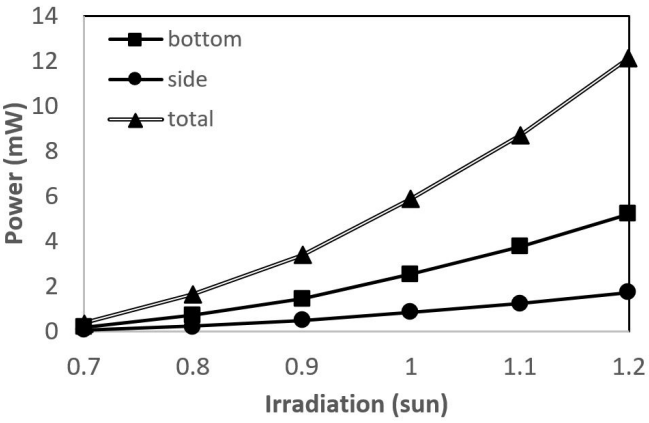


**Fig. 7. Maximum generated power by TEG modules (four on each side and four on the bottom side and total of 20 TEGs for the hybrid system) at the different radiation levels**

It can be seen that as the solar irradiance rises, the generated power increases at a growing rate. The radiation varies from 700 to 1200 W/m$^2$ and the generated power increases from 0.37 mW to 12.1 mW. The comparison between generated power by downside and side TEGs depicts that by increasing 4˚C in surface temperature, the produced power has been tripled which reveals that the temperature difference is the major parameter for thermoelectric power generation.
Moreover, Fig. 8 shows the ratio of the power generated by four TEG to the power generated by the PV module for the bottom face. It is shown that by increasing the irradiation level, this value increases too. The growth rate for the bottom face is more than the side faces. By increasing the radiation level, this value reaches about 2% at the maximum radiation level of 1200 W/m$^2$. By analyzing Figs. 6 to 8 simultaneously, one can conclude that the best configuration for the hybrid cavity is the hybrid PV-TEG modules on the downside surface and the TEG modules on the side surfaces.

### 3- 2- Aperture size effect

Aperture size has a significant effect on reducing the re-radiation loss from cavity opening. Figs. 9 (a) and 9 (b) show the cross-section of the cavity receiver with a small size

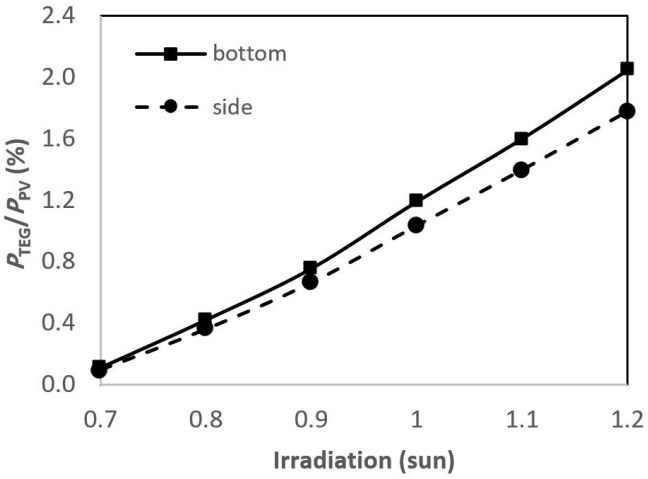


**Fig. 8. The ratio of generated power by TEG modules to generated power by PV modules at various irradiation levels**

aperture. In this study, the aperture opening ratio is defined as the ratio of cavity opening area (*a* dimension) to cavity surface area (*b* dimension). The effect of aperture size is investigated by comparing fully open aperture cavity and 45% opening aperture area (5×5 cm$^2$ aperture).

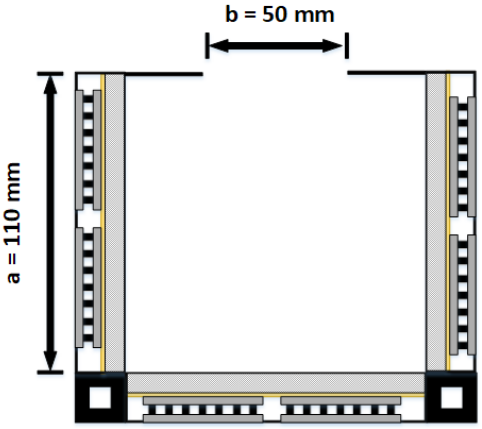


(a)

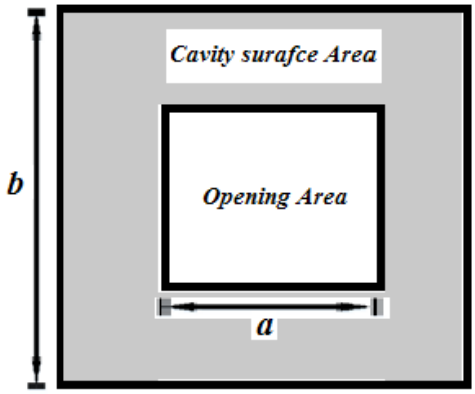


(b)

**Fig. 9. The Cross-section of a square cavity-receiver (a) with a 5×5 cm$^2$ aperture (b) opening aperture area**

The temperature variation of the bottom and side surfaces of the cavity with 5×5 cm$^2$ ($a/b$=0.45) aperture is shown in Figs. 10 (a) and 10 (b).

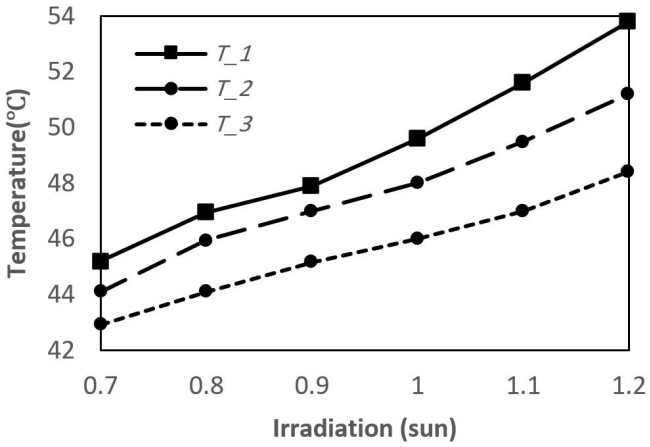


(a)

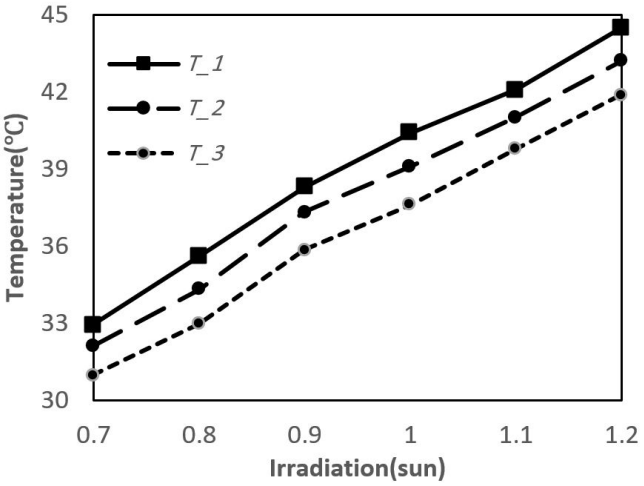


(b)

**Fig. 10. Temperature variation of the cavity with opening aperture ratio 45% ($a/b$=0.45) at various solar radiation levels for (a) the bottom face (b) the side faces**

As temperature variation trend at different levels of irradiation shows, by decreasing the cavity aperture size, the input irradiation from the aperture to cavity surfaces is reduced. Consequently, the surface temperature of the PV surface on the bottom side for the small aperture cavity is lower than the open aperture cavity one, as it is shown in Fig. 11. The temperature difference of bottom face for two cavity aperture types is calculated for different irradiation levels. As Fig. 11 depicts, in the fully open cavity ($a/b$=1), the temperature increases with a steeper slope than the cavity with the smaller aperture ($a/b$=0.45). The thermoelectric power generation is dependent on the temperature difference a great deal. Therefore, the application of small cavity causes the TEG power generation reduction. On the other hand, the best performance of the PV modules occurs at low working temperatures. Therefore, the decision about the selection of the cavity type with higher efficiency will depend on the level of generated power of hybrid, which is presented by Figs. 12 and 13.

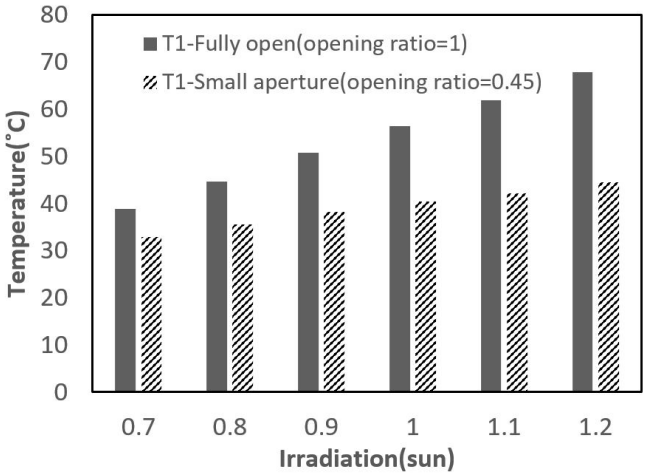


**Fig. 11. Bottom surface temperature comparison between the small aperture ($a/b$=0.45) cavity and fully open cavity ($a/b$=1)**

Variation of the maximum generated power via the PV modules and via the TEG modules on each side of a cavity with the aperture size of 5×5 cm$^2$ ($a/b$=0.45) versus irradiation are given in Figs. 12 (a) and 12 (b) respectively.

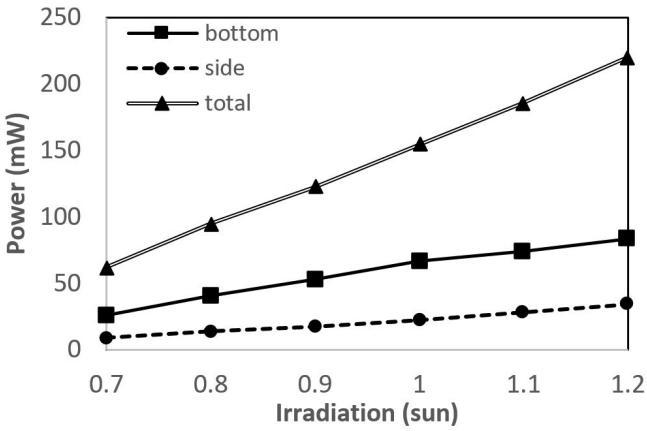


(a)

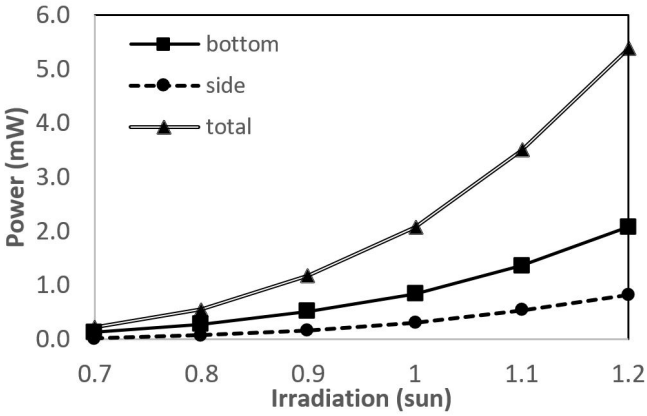


(b)

**Fig. 12. (a) Maximum generated power of the cavity with the opening ratio of 0.45 at various radiation levels by (a) the PV modules, (b) TEG modules (Four on each side and four on the bottom and the total 20 TEGs of the hybrid system)**

The total power generation of the hybrid cavity with the aperture ratio of 0.45 and fully open aperture is compared in Fig. 13. The generated power ratio is calculated by dividing the generated power of fully open cavity to the generated power of small aperture cavity. Fig. 13 shows the power ratio of two aperture types differ at various irradiation levels and decreases from 6 to 3 by increasing the irradiation level from 0.7 to 1.2 sun. The 50% reduction in generated power ratio shows that the effect of aperture size on the reduction of re-radiation loss from the cavity. However, the re-radiation loss at higher irradiation levels increases. Therefore, the application of smaller aperture is more efficient at higher irradiation levels.

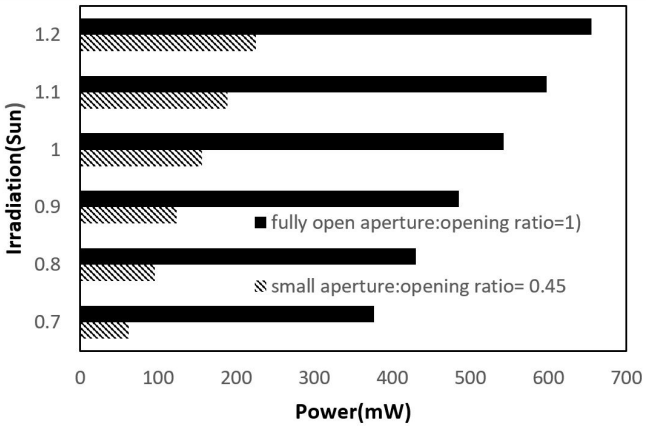


**Fig. 13. The total generated power for two different type cavity apertures at various irradiances**

Although applying the small size aperture reduces the re-radiation and increases the efficiency of the system, however, it will decrease the total produced power because of reduction in input irradiance. The efficiency of fully open and 5×5 $cm^2$ aperture is presented in Fig. 14. The results show that by reducing the opening ratio from 100% to 45%, the efficiency improves by 27%.

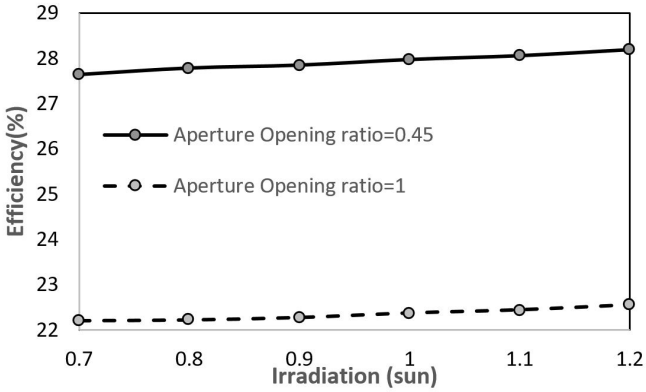


**Fig. 14. Efficiencies of the hybrid system (fully open aperture (opening ratio=1) and small aperture with opening ratio=0.45) at various irradiances**

### 3- 2- 1- Aperture size optimization

The discussions about aperture size effect in section 3.2 depict that by applying smaller aperture size, the input radiation to the cavity and the re-radiation loss from cavity are reduced. Moreover, significant loss reduction occurs at higher irradiation levels. These rising and reduction trends are investigated by absorption ability of the cavity. The absorption efficiency of cavity receiver is given by the Eq. (22) [28]:

$$\eta_{absorption} = \frac{\alpha_{eff} P_{aperture} - \epsilon_{eff} A_{aperture} T^4}{Q_{solar}} \quad (22)$$

where $\alpha_{eff}$, $\epsilon_{eff}$ are effective absorptance and emittance of the cavity, $P_{aperture}$ is radiation input to the cavity from the aperture, $Q_{solar}$ is total irradiation power on the cavity surface, $A_{aperture}$ is the aperture area, and $T$ is the nominal temperature of the cavity. The Gaussian power flux distribution on the cavity top surface and aperture is assumed. $\alpha_{eff}$ and $\epsilon_{eff}$ are calculated as discussed in Fig. 2 when the aperture size changes from 1cm to 11cm. Figs. 15, 16 (a), and 16 (b) present the absorption efficiency of a cubic cavity when the aperture opening ratio varies from 0.1 to fully open (aperture size varies from 1 cm to 11cm) and irradiation changes from 0.7 to 1.2 sun. As Fig. 16 (a) shows, the maximum efficiency of about 96% occurs at the minimum irradiation level. The difference between the maximum and minimum efficiency at the different irradiation levels, changes from 0.22% for the aperture size of 1 cm to 5.3% for the aperture size of 11 cm which is presented in Fig.16 (b). The absorption efficiency figure follows a similar trend at small and full aperture sizes. For the small aperture size, the absorption efficiency is very low. It is due to the slight input radiation to the cavity and due to the increase in the re-radiation loss. The full aperture cavity follows the same trend as the aperture size increases. Consequently, by balancing between the minimum re-radiation and maximum irradiation, there is one optimum aperture size that the absorption efficiency reaches the maximum value.

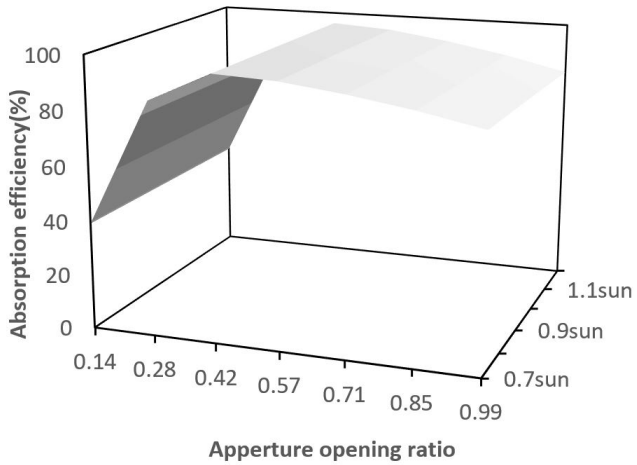


**Fig. 15. Absorption efficiency of the cavity with various aperture ratio, under different solar irradiation level**

Fig. 17 shows the maximum absorption efficiency value for different irradiant level versus aperture opening ratio. The absorption efficiency of 11×11×11 $cm^3$ cubic cavity is calculated under irradiation level 0.7 to 1.2 sun, and the optimum size of the square aperture with maximum absorption and minimum re-radiation loss is 4.7 cm with opening ratio 0.43 as shown in Fig. 17.

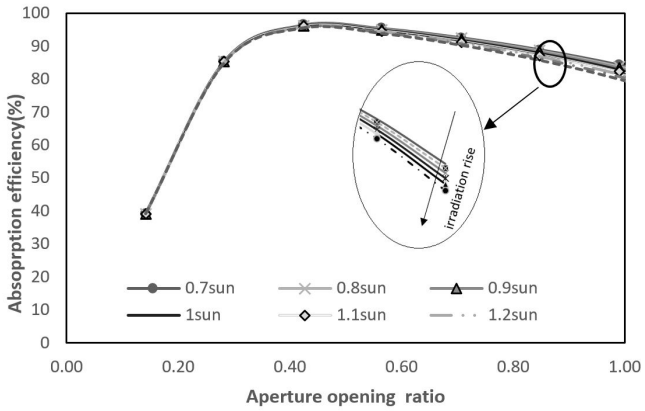


(a)

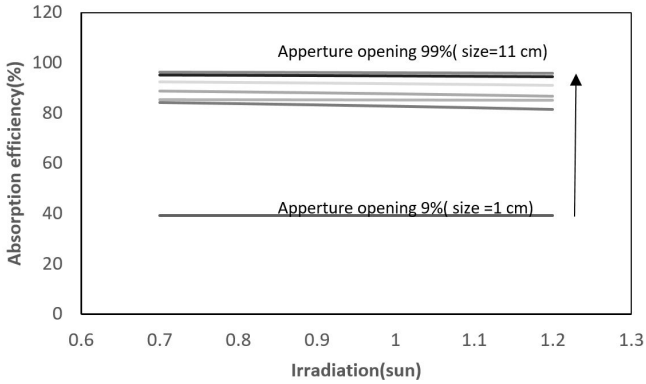


(b)

**Fig. 16. Radiation absorption efficiency of cubic cavity versus (a) various aperture opening ratio (b) different solar irradiation level**

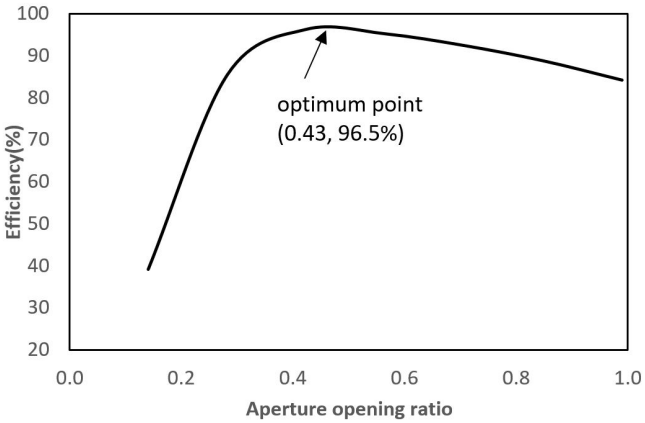


**Fig. 17. Maximum absorption efficiency of the cubic cavity for various aperture opening ratio under different solar irradiation level**

## 4- Conclusion

In the present paper, a hybrid photovoltaic-thermoelectric power generating system using a cubical cavity receiver is proposed and simulated via the numerical method. The PV modules are placed inside the cavity, and the TEGs are attached backside of them. It is shown that higher radiation levels which would result not only in larger PV generated power but also in higher temperature difference through the TEG module lead to a higher TEG power generated. Moreover, it is shown that at 1000 W/m$^2$ irradiance, the hybrid system with 5 PV module and 20 TEG module can produce 536 mW which is 2.4 times the PV-TEG alone. Other simulations are also performed to evaluate the performance of the system for cavities with smaller aperture size (opening ratio<1). The result showed that reducing the aperture size, decrease obtained radiation input and so the mean temperature of the system decreases. On the other hand, using closer aperture causes the reduction in re-radiation loss and so the system efficiency rises from 22% to 28%. Although the smaller aperture size increases the system efficiency, however, due to the reduction in input radiation, the output power decreases. The optimum size of cavity aperture by balancing between less re-radiation and higher irradiation absorption is calculated. The optimization result shows that the optimum opening ratio of the aperture is 42.7% under different irradiation level. Consequently, for the 11×11×11 cm$^3$ cubic cavity at irradiation levels from 0.7 to 1.2 sun, the optimum size of the square aperture is 4.7 cm. Regarding the power generated of the bottom and side PV modules, it is suggested to have only TEG modules on side walls since the configuration of the side PV modules leads to a lower attraction of irradiance and lower power generated.

## Acknowledgments

The authors would like to express very great appreciation to Prof. Farshad Kowsari for his valuable and constructive suggestions during the planning and development of this research work. His willingness to give his time so generously has been very much appreciated.

## Nomenclature

| | |
|---|---|
| $a$ | Baseline dimension |
| $b$ | Aperture width |
| $F_{i-j}$ | View factor |
| $G_{ref}$ | Reference radiation level |
| $G$ | Available radiation flux on the PV module |
| $g$ | Gravitational acceleration |
| $I_o$ | The saturation current |
| $I_{ph,ref}$ | Reference photocurrent |
| $L$ | Characteristic length-scale of convection |
| $Nu$ | Nusselt number |
| $P_{TEG,max}$ | maximum power generated by the TEG |
| $q_o$ | Radiosity flux |
| $Q$ | Heat transfer |
| $R_i$ | Internal electrical resistance |
| $R_{pv}$ | Thermal resistance of PV module |
| $Ra$ | The Rayleigh number |
| $S$ | Seebeck coefficient, |
| $T_{air}$ | Air temperature |
| $T_{1,k}$ | Temperature of inside cavity of the $k^{th}$ surface |
| $T_{2,k}$ | Temperature of hot plate of the kth surface |
| $T_{3,k}$ | Temperature cold plate of the kth surface |

| | |
|---|---|
| $T_{ref}$ | Reference temperature of PV modules |
| $k_{air}$ | Air conductivity |
| $RL$ | Load resistance |

**Greek symbols**

| | |
|---|---|
| $\mu_I$ | Temperature coefficient of current |
| $\mu_{air}$ | Air dynamic viscosity |
| $\mu_V$ | Open-circuit voltage temperature coefficient |
| $\beta$ | Coefficient of thermal expansion |
| $\vartheta$ | Kinematic viscosity, |
| $\alpha$ | Thermal diffusivity |
| $\varepsilon$ | Surface emissivity |
| $\sigma$ | Stefan–Boltzmann's constant |

## References


[1] A.A.J. Muto, *Thermoelectric device characterization and solar thermoelectric system modeling*, Massachusetts Institute of Technology, 2011.

[2] J. Tonui, Y. Tripanagnostopoulos, Performance improvement of PV/T solar collectors with natural air flow operation, *Solar Energy*, 82(1) (2008) 1-12.

[3] G. Rockendorf, R. Sillmann, L. Podlowski, B. Litzenburger, PV-hybrid and thermoelectric collectors, *Solar Energy*, 67(4-6) (1999) 227-237.

[4] W. He, J. Zhou, C. Chen, J. Ji, management, Experimental study and performance analysis of a thermoelectric cooling and heating system driven by a photovoltaic/thermal system in summer and winter operation modes, *Energy conversion and management*, 84 (2014) 41-49.

[5] L. Tayebi, Z. Zamanipour, D. Vashaee, Design optimization of micro-fabricated thermoelectric devices for solar power generation, *Renewable Energy*, 69 (2014) 166-173.

[6] D. Kossyvakis, G. Voutsinas, E. Hristoforou, Management, Experimental analysis and performance evaluation of a tandem photovoltaic–thermoelectric hybrid system, *Energy Conversion and Management*, 117 (2016) 490-500.

[7] Y. Vorobiev, J. González-Hernández, P. Vorobiev, L. Bulat, Thermal-photovoltaic solar hybrid system for efficient solar energy conversion, *Solar Energy*, 80(2) (2006) 170-176.

[8] E. Chávez-Urbiola, Y.V. Vorobiev, L. Bulat, Solar hybrid systems with thermoelectric generators, *Solar energy*, 86(1) (2012) 369-378.

[9] H. Najafi, K.A. Woodbury, Modeling and analysis of a combined photovoltaic-thermoelectric power generation system, *Journal of Solar Energy Engineering*, 135(3) (2013) 031013.

[10] S. Soltani, A. Kasaeian, H. Sarrafha, D. Wen, An experimental investigation of a hybrid photovoltaic/thermoelectric system with nanofluid application, *Solar Energy*, 155 (2017) 1033-1043.

[11] Y. Deng, W. Zhu, Y. Wang, Y. Shi, Enhanced performance of solar-driven photovoltaic–thermoelectric hybrid system in an integrated design, *Solar energy*, 88 (2013) 182-191.

[12] J. Zhang, Y. Xuan, L. Yang, Performance estimation of photovoltaic–thermoelectric hybrid systems, *Energy*, 78 (2014) 895-903.

[13] X. Ju, Z. Wang, G. Flamant, P. Li, W. Zhao, Numerical analysis and optimization of a spectrum splitting concentration photovoltaic–thermoelectric hybrid system, *Solar Energy*, 86(6) (2012) 1941-1954.

[14] J. Zhang, Y. Xuan, L.Yang, A novel choice for the photovoltaic–thermoelectric hybrid system: the perovskite solar cell, *International Journal of Energy Research*, 40(10) (2016) 1400-1409.

[15] F. Willars-Rodríguez, E. Chávez-Urbiola, P. Vorobiev, Y.V. Vorobiev, Investigation of solar hybrid system with concentrating Fresnel lens, photovoltaic and thermoelectric generators, *International Journal of Energy Research*, 41(3) (2017) 377-388.

[16] H. Najafi, K.A. Woodbury, Optimization of a cooling system based on Peltier effect for photovoltaic cells, *Solar Energy*, 91 (2013) 152-160.

[17] Y.-Y. Wu, S.-Y. Wu, L. Xiao, Management, Performance analysis of photovoltaic–thermoelectric hybrid system with and without glass cover, *Energy Conversion and Management*, 93 (2015) 151-159.

[18] C. Suter, P. Tomeš, A. Weidenkaff, A. Steinfeld, A solar cavity-receiver packed with an array of thermoelectric converter modules, *Solar Energy*, 85(7) (2011) 1511-1518.

[19] J.R. Howell, M.P. Menguc, R. Siegel, *Thermal radiation heat transfer*, CRC press, 2015.

[20] S. Lin, E. Sparrow, Radiant interchange among curved specularly reflecting surfaces—application to cylindrical and conical cavities, *Journal of Heat Transfer*, 87(2) (1965) 299-307.

[21] A. Steinfeld, Apparent absorptance for diffusely and specularly reflecting spherical cavities, *International journal of heat and mass transfer*, 34(7) (1991) 1895-1897.

[22] J.R. Howell, *Catalog of Radiation Heat Transfer Configuration Factors*, in, 2010.

[23] J.F. Hinojosa, C.A. Estrada, Three-dimensional numerical simulation of the natural convection in an open tilted cubic cavity, *Revista mexicana de física*, 52(2) (2006) 9.

[24] D. I. f. P. Properties, *DIPPR Project* 801 in: D.I.f.P.P. Research/AIChE (Ed.), 2010.

[25] D.M. Rowe, *CRC Handbook of Thermoelectrics*, CRC Press, 1995.

[26] E. Saloux, M. Sorin, Explicit model of photovoltaic panels to determine voltages and currents at the maximum power point, *Solar Energy*, 85(5) (2011) 10.

[27] O. Farhangian Marandi, M. Ameri, B. Adelshahian, The experimental investigation of a hybrid photovoltaic-

thermoelectric power generator solar cavity-receiver, *Solar Energy*, 161 (2018) 38-46.

[28] A. Steinfeld, Optimum aperture size and operating temperature of a solar cavity-receiver Solar Energy, 50(1) (1993) 7.

Please cite this article using:

O. Farhangian Marandi, M. Ameri, B. Adelshahian, Modeling and Analysis of a Hybrid Photovoltaic-Thermoelectric Solar Cavity-Receiver Power Generator, *AUT J. Mech. Eng.*, 2(2) (2018) 277-288.

DOI: 10.22060/ajme.2018.14018.5698